GaN and SiC Based 500kHz Resonant Bidirectional DC/DC Design for 800V OBCM Application

Minli Jia
Shanghai EV Design Center
Navitas Semiconductor
Shanghai, China
minli.jia@navitassemi.com

Hao Sun
Shanghai EV Design Center
Navitas Semiconductor
Shanghai, China
hao.sun@navitassemi.com

Jingxian Cai
Shanghai EV Design Cente
Navitas Semiconducto)
Shanghai, China
jingxian.cai@navitassemi.com

Haisong Zhang
Shanghai EV Design Center
Navitas Semiconductor
Shanghai, China
hanson.zhang@navitassemi.com

Zhen Zhou
Shanghai EV Design Center
Navitas Semiconductor
Shanghai, China
zhen.zhou@navitassemi.com

Jinlong Chen
Shanghai EV Design Center
Navitas Semiconductor
Shanghai, China
jinlong.chen@navitassemi.com

***Abstract*—A 6.6kW 500kHz bidirectional isolated DC/DC converter based on GaN and SiC wide band gap (WBG) semiconductor devices is developed for 800V electric vehicle (EV) on-board charging, which is simpler and more reliable than the method of 800V output using multilevel topology. Firstly, the working characteristics of resonant DAB topology using phase-shift control are analyzed. Compared with the delay-time control strategy, it has the factures of narrow switching frequency range and small turn-off current, which is very suitable for high frequency applications of SiC devices. Secondly, a magnetic integrated high-frequency transformer was designed, and Maxwell software was adopted for simulation, comparison, and optimization. Compared with the traditional 90kHz transformer design, the volume was reduced by about 50%. Thirdly, based on the specifications of EV on-board charger, the loss breakdown calculation of the worst-case working condition of charging and discharging mode is carried out to verify the rationality of the design. Finally, based on water-cooled heat dissipation, a 500kHz 6.6kW 800V bidirectional DC/DC experimental platform was built. The full power output voltage range is form 550V to 900V, and the peak efficiency more than 98% at normal temperature, which verified the feasibility of the high-frequency hybrid application design of GaN and SiC devices.**

Keywords—On Board Charger, High-frequency, GaN, SiC

I. INTRODUCTION

In recent years, with the explosive growth of EVs, the competition is intensifying, and the on-board power conversion units of EV are developing in the direction of high frequency, high efficiency and high power density, which provides opportunities for the application of WBG semiconductors GaN and SiC.

On-board charger module (OBCM) is an important energy conversion component of EVs, which not only has the function of charging the vehicle battery, but also has the function of discharging, which can realize a variety of applications such as vehicle-to-load (V2L), vehicle-to-grid (V2G) and vehicle-to-home (V2H). As an important part of the OBCM, bidirectional DC/DC (Fig.1(a)) plays the function of electrical isolation and voltage regulation, which can be combined with wide band gap semiconductor devices and ZVS switching control to achieve high frequency and high efficiency design. For the application of GaN devices in OBCM, many scholars have done a lot of research on topology, control, etc. [1]. Since the voltage withstand of GaN devices is 650V, its application in 800V battery voltage system must use series half-bridge (SHF), three-level neutral point clamped (NCP) or three-level flying-capacitor (FC) topology (Fig.1(b)), the corresponding control, component number and drive design are relatively complex. SiC devices can withstand up to 1200V and have been used in 800V systems, but the product application of 500kHz is still relatively rare, which is the research background of this paper.

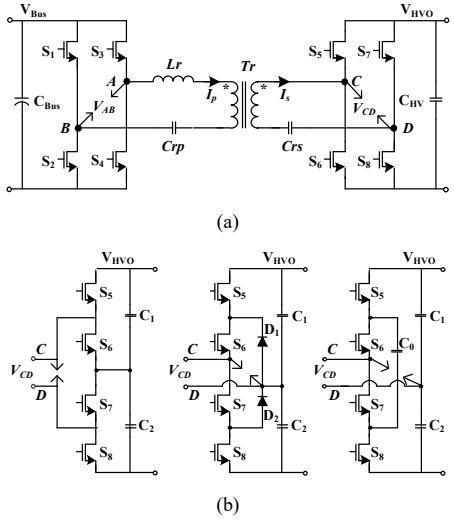

Fig. 1. GaN based 400V and 800V bidirectional dc/dc topology.(a) is the topology for 400V system and (b) is the topology for 800V system

Bidirectional DC/DC usually refers to dual-active-bridge (DAB) topology, which is divided into resonant type and non-resonant type. Literature [2], [3], [4], [5] based on resonant CLLC design, zero-voltage-switching (ZVS) with high switching frequency is very suitable for the application of GaN and SiC. However, to obtain the output with wide gain, the input bus voltage must be adjusted in a wide range, and the selection of high-voltage bus capacitors will increase the volume and cost. Literature [6] ,[7]proposes a Delay-time control method, which realizes wide gain adjustment of output and switches ZVS action by controlling the short-circuit state of the transformer's secondary side. However, the switching frequency sometimes reaches more than 2 times of the resonant frequency during the actual design, resulting in turn-off loss increased and efficiency reduced. Literature [8] summarizes the topology and control of DAB circuits. To expand the switching range of ZVS, scholars have successively proposed extended-phase-shift (EPS), dual-phase-shift (DPS) and triple-phase-shift (TPS) control

methods based on traditional single-phase-shift (SPS) control, further expanding the application of DAB topology. To further reduce the turn-off loss, literature [9], [10] combined fixed frequency control with LC resonant network to ensure that the turn-off current of ZVS switching is further reduced and adopted frequency conversion and phase shift control to achieve a wide range of voltage output. Based on this topology, this paper will study 800V output voltage combined with GaN and SiC devices.

High frequency transformers use PCB winding [11] or Litz wire winding and combined with magnetic integrated technology [12] can minimize the volume. High frequency and high-power applications are usually based on Litzi wire winding design, PCB solutions are less used because of the skin effect of current increases with the frequency increasing, and the equivalent AC impedance becomes larger. In addition, the magnetic integrated design of leakage inductance as a resonant inductor can achieve the optimal volume [13], [14],[15], but the winding arrangement should be comprehensively considered to reduce AC impedance and loss.

The structure of this paper is as follows: Firstly, the principle of resonant DAB is analyzed; secondly, the Maxwell simulation model of high-frequency integrated transformer is designed and comparison; finally, the feasibility of SiC devices high-frequency application is verified based on the 800V 6.6kw 500khz bidirectional DC/DC converter platform of water-cooled heat dissipation.

II. TOPOLOGY AND CONTROL

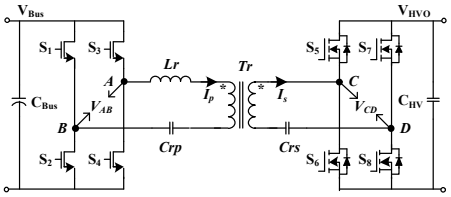

Fig. 2. Topology of resonant DAB

Fig. 2 shows the topology configuration of resonant DAB. S_1~S_4 are primary side switches. Since the V_{Bus} voltage is 400V, 650V GaN devices are used. S_5~S_8 are secondary side switches, V_{HVO} is 800V, 1200V SiC devices are used. Tr is the high frequency isolation transformer, Lr is the resonant inductor, Crp and Crs are the primary and secondary resonant capacitors respectively. C_{Bus} and C_{HV} are the bus side and the high voltage output side capacitors respectively.

A. Working Mode Analysis

The key waveforms of SPS control resonant DAB are shown in Fig. 3. S_2/S_3 and S_1/S_4 of the primary side drive are complementary, and S_5/S_8 and S_6/S_7 of the secondary side drive are also complementary. The output voltage is controlled by the phase-shift of the primary and secondary sides. Eight operating modes in a switching cycle, because of the positive and negative half-cycle symmetry, this paper only analyzes the four modes of the resonant current positive half-cycle.

Working mode 1 [t_0~t_1]: Before t_0 of the resonant current crossing, S_3 and S_2 have been ZVS turn-on, the input voltage V_{AB} and the equivalent output voltage n*V_{CD} are connected in series to excite the resonant tank, and Lr stores energy. The larger the phase-shift angle α in this period, the more Lr energy storage, the higher output gain of the system. Fig. 4 shows the corresponding current flow diagram and equivalent circuit. Cr is the equivalent resonant capacitor, and satisfied: $Cr = Crp(Crs/n^2)/(Crp + Crs/n^2)$.

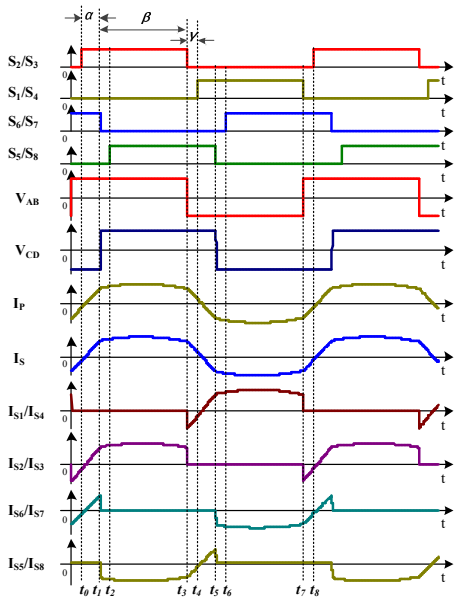

Fig. 3. Key waveforms of a switching cycle

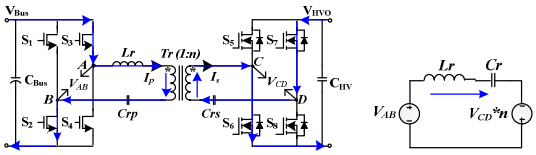

Fig. 4. Working mode 1 and its equivalent circuit

Working mode 2 [t_1~t_2]: at t_1, S_6 and S_7 are turn-off, the secondary side devices of the transformer enter the dead-time, the resonant current is rectified through the body diode of S_5 and S_8, and the input transmits energy to the output. Fig. 5 is the current flow diagram and equivalent circuit.

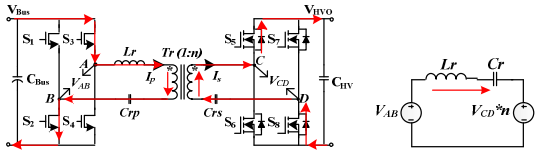

Fig. 5. Working mode 2 and its equivalent circuit

Working mode 3 [t_2~t_3]: At t_2, S_5 and S_8 ZVS turn-on, the secondary side devices enter the synchronous rectifier state, and the input continues to transfer energy to the output. The state is the same as that of working mode 2. Fig. 6 is the corresponding current flow diagram and equivalent circuit.

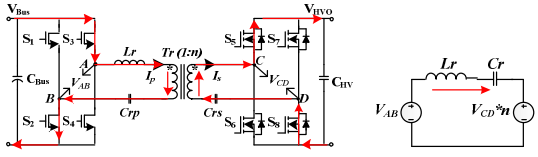

Fig. 6. Working mode 3 and its equivalent circuit

Working mode 4 [t_3~t_4]: At t_3, S_2 and S_3 are turn-off, DAB primary side resonant current continues to flow through the body diodes of S_1 and S_4, the primary side voltage source of the resonator tank is reversed, and the energy in the inductor is fed back to the primary side to prepare for the soft switch at the next moment, on the other hand, the resonant tank continues to transfer energy to the load. This mode corresponds to Angle γ. Fig. 7 shows the corresponding current flow diagram and equivalent circuit.

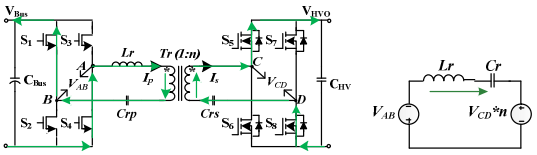

Fig. 7. Working mode 4 and its equivalent circuit

B. Phase Plane Analysis

According to the above working mode analysis, there are three equivalent working modes in half a switching cycle, as shown in Fig. 8. This paper defines the three modes corresponding to angles α, β and γ respectively. Phase plane analysis method was adopted, as shown in Fig. 9.

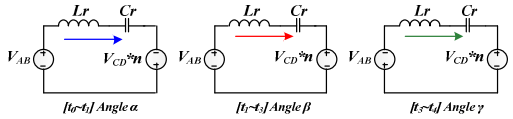

Fig. 8. Three equivalent circuit in half switching cycle

All parameters are normalized based on V_{Bus} as follows :

- Input voltage: $M_g = V_{Bus}/V_{Bus} = 1$
- Output voltage: $M_g = n * V_{HVO}/V_{Bus}$
- Voltage of Cr: $m_c = V_{CR}/V_{Bus}$
- Peak voltage of Cr: $M_{RP} = V_{CR_{PEK}}/V_{Bus}$
- Resonant current: $j_L = i_{Lr} R_0/V_{Bus}$

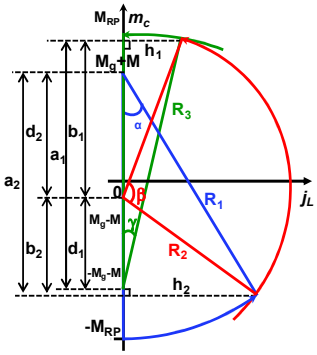

Fig. 9. Phase plan analysis of half switching cycle

Where, R_0 is the characteristic impedance and expressed as: $R_0 = \sqrt{Lr/Cr}$.

According to geometric relations in Fig. 9, $d_1=2M_g$, $d_2=2M$, $R_1=M_{RP}+M_g+M$, $R_3=M_{RP}+M+M_g$, and other expressions can be solved as follows:

$$\begin{cases} a_1 - b_1 = d_1 \\ a_1^2 + h_1^2 = R_3^2 \\ b_1^2 + h_1^2 = R_2^2 \\ a_2 - b_2 = d_2 \\ a_2^2 + h_2^2 = R_1^2 \\ b_2^2 + h_2^2 = R_2^2 \end{cases} \tag{1}$$

$$a_1 = \frac{R_3^2 - R_2^2 + d_1^2}{2d_1} \tag{2}$$

$$h_1 = \sqrt{R_3^2 - a_1^2} \tag{3}$$

$$a_2 = \frac{R_1^2 - R_2^2 + d_2^2}{2d_2} \tag{4}$$

$$h_2 = \sqrt{R_1^2 - a_2^2} \tag{5}$$

The α Angle can be obtained as:

$$\alpha = sin^{-1}\frac{h_2}{R_1} \tag{6}$$

The β starting Angle is:

$$\beta_{start\_angle} = sin^{-1}\frac{h_2}{R_1} \tag{7}$$

The γ Angle can be obtained as:

$$\gamma = \sin^{-1}\frac{h_1}{R_3} \tag{8}$$

The β Angle can be obtained as:

$$\beta = \pi - sin^{-1}\frac{h_2}{R_1} - sin^{-1}\frac{h_1}{R_3} \tag{9}$$

Finally, the expression of resonant current can be obtained as follows, the waveform of each part can be derived from this formula.

$$I_{Lr}(t) = \begin{cases} \frac{V_g}{R_0}[R_1\sin(\omega t)] & 0 \le t < T_\alpha \\ \frac{V_g}{R_0}\{R_2\sin[\omega(t-T_\alpha)+\beta_{start\_angle}]\} & T_\alpha \le t < T_\alpha + T_\beta \\ \frac{V_g}{R_0}\{R_3\sin[\omega(t-T_\alpha-T_\beta)+\pi-\gamma]\} & T_\alpha + T_\beta \le t \le \frac{T_s}{2} \\ -\frac{V_g}{R_0}\left[R_1\sin\omega\left(t-\frac{T_s}{2}\right)\right] & \frac{T_s}{2} \le t < \frac{T_s}{2} + T_\alpha \\ -\frac{V_g}{R_0}\left\{R_2\sin\left[\omega\left(t-\frac{T_s}{2}-T_\alpha\right)+\beta_{start\_angle}\right]\right\} & \frac{T_s}{2} + T_\alpha \le t < \frac{T_s}{2} + T_\alpha + T_\beta \\ -\frac{V_g}{R_0}\left\{R_3\sin\left[\omega\left(t-\frac{T_s}{2}-T_\alpha-T_\beta\right)+\pi-\gamma\right]\right\} & \frac{T_s}{2} + T_\alpha + T_\beta \le t \le T_s \end{cases} \tag{10}$$

C. Comparision with Delay-time Control

Resonant DAB and delay-time Boost SRC control have the similar control strategies [6] ,[7], but they are different. As shown in Table I, the items of modulation strategy, α angle excitation source, switching frequency, turn-off current of secondary side devices, control methods and output ripple current are compared. Resonant DAB has advantages in control, turn-off current, turn-off loss, etc., especially its small turn-off current, which provides the possibility for high frequency applications of SiC devices.

TABLE I. RESONANT DAB VS DELAY-TIME CONTROL

Items	Comparison	
	Resonant DAB control	***Delay-time control***
Secondary side Modulation Strategy	Active control	Active + SR control
Control	Phase-shift	Variable frequency + delay-time
Excitation source	V_{AB} and n* V_{CD}	V_{AB}
Switching frequency range	Small	Large
Turn-off current of secondary side device	Low	High
Output ripple current	large	small

Under the same working conditions, the waveform of resonant current of resonant DAB and delay-time control Boost SRC can be obtained according to formula (10) and literature [7] respectively, as shown in Fig. 10. It can be seen that the turn-off current controlled by resonant DAB is nearly 2 times smaller than that controlled by delay-time.

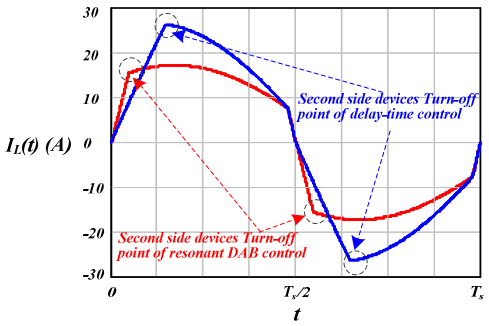

Fig. 10. Comparison of resonant current between resonant DAB and delay-time control Boost SRC

III. HIGH FREQUENCY TRANSFORMER DESIGN

The resonant inductor and the isolation transformer are the two main magnetic components in resonant DC/DC converter. The integrated design can reduce the volume and improve the power density. There are two integrated implementation methods, one is that the resonant inductor fully utilizes the leakage inductance of the transformer, which is a fully magnetic integrated design. The other is the partial leakage and independent inductance integration, is a partial integration of the design, both have their own characteristics.

A. Full Integration Transformer Design

The design principle of the fully integrated transformer is to match the leakage inductance by adjusting the coupling coefficient of the primary and secondary sides. The smaller the coupling coefficient, the greater the leakage inductance, but it will lead to the enhancement of the winding current skin effect, and then lead to the increase of the AC loss of the winding. In this paper, the design analysis is based on the winding arrange of PSPSP with multiple interleaving of primary and secondary sides, and the section of the central column of the magnetic core is assumed to be ideally circular, as shown in Fig. 11, where E and D are the radius of the central column and the inner window of the magnetic core respectively. Due to the symmetry of the structure, only half of the magnetic core is analyzed and calculated for leakage induction. X, Y, Z, M and N represent the winding width of the coil and the gap width between the coils, respectively, and H is the spatial magnetic field distribution.

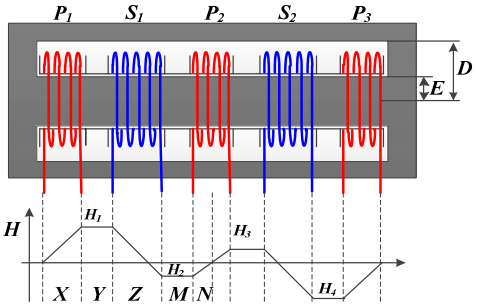

Fig. 11. Structure of integrated magnetic transformer

The window area for storing leakage energy is:

$$A_W = \pi(D^2 - E^2) \tag{11}$$

The total magnetic field of the window space is:

$$H = 2\frac{N_P \cdot I_P}{D - E} \tag{12}$$

Where, Np and Ip are the number of primary side turns and resonant current respectively.

According to the electromagnetic field theory, the electric field strength of X, Y, Z, M and N regions can be expressed as:

$$E_X = \int_0^x \frac{1}{2}\mu_0 \cdot \left(\frac{H_1 \cdot x}{X}\right)^2 \cdot A_W \cdot \mathrm{d}x \tag{13}$$

$$E_Y = \frac{1}{2}\mu_0 \cdot {H_1}^2 \cdot Y \cdot A_W \tag{14}$$

$$E_Z = \int_0^z \frac{1}{2}\mu_0 \cdot \left(H_1 - \frac{H_1 \cdot z}{Z}\right)^2 \cdot A_W \cdot \mathrm{d}z \tag{15}$$

$$E_M = \frac{1}{2}\mu_0 \cdot {H_2}^2 \cdot M \cdot A_W \tag{16}$$

$$E_N = \int_0^z \frac{1}{2}\mu_0 \cdot \left(H_2 - \frac{H_2 \cdot n}{N}\right)^2 \cdot A_W \cdot \mathrm{d}n \tag{17}$$

The total electric field intensity satisfies the following relation:

$$E = 2(E_X + E_Y + E_Z + E_M + E_N) \tag{18}$$

According to the Faraday's law of induction:

$$E = \frac{1}{2} \cdot L_K \cdot {I_P}^2 \tag{19}$$

Combining (18) and (19), the leak inductance Lk can be expressed as:

$$L_K = \frac{4(E_X + E_Y + E_Z + E_M + E_N)}{{I_P}^2} \tag{20}$$

From above analysis, it can be found that the value of leakage inductance depends on X, Y, Z, M, N, Np and Ip after the core size is determined.

B. Simulation and Optimization Design

The transformer turns ratio designed is 12:20, leakage inductance is 6uH, and the winding distribution of the transformer designed is shown in Fig. 12. According to the above formula (20), the leakage inductance value calculated is 6.1uH, and the maxwell 2D simulation leakage inductance value is 6.8uH. The two results are close. The correctness of the above analysis is verified.

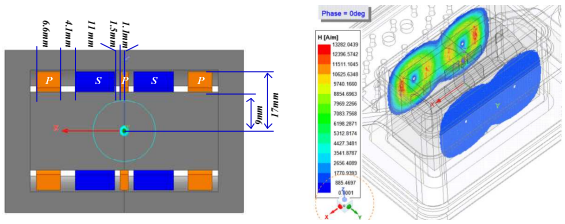

Fig. 12. PSPSP winding arrange and Distribution of magnetic leakage on the shell

For OBCM applications, water-coolant heat dissipation is adopted. The transformer is enclosed in the aluminum shell, and eddy current loss is caused by the leakage magnetic field in the metal shell. When the distance between the transformer and the aluminum shell is 3mm, Maxwell 3D simulated distribution of the leakage magnetic field in the metal shell is shown in Fig. 12. There are usually two solutions: one is to increase the distance between the leakage magnetic field and the metal side wall, but it will lead to an increase in the volume of the product; The other is to reduce the gap of the primary and secondary side winding, but it will lead to the reduction of leakage inductance. Therefore, when designing, resonant inductance will be realized by transformer leakage inductance add external independent inductance.

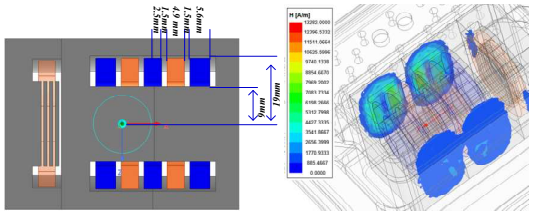

Fig. 13. SPSPS winding arrange and Distribution of magnetic leakage on the shell

The optimized transformer structure design of SPSPS winding arrange is shown in Fig. 13. The primary and secondary side winding gap is 1.5mm and additional loss caused by magnetic leakage in the metal shell is reduced. At the same distance of 3mm from the shell, it can be seen from the cloud image distribution of H in the shell that the magnetic field significantly weakens. The partial of resonant inductance is supplemented by an independent inductor, which adopts a segmented air gap design to reduce the AC loss of inductor windings. According to Maxwell 3D simulation, the transformer's own leakage inductance is 2.15uH, the independent inductance is 4uH, and the total leakage inductance is 6.15uH, meeting the requirements.

IV. Simulation and Experimental Verification

The design parameters of bidirectional resonant DAB are shown in Table II: The bus side voltage range is 360~420V, the high-voltage side voltage range is 550~900V, the power of charging mode is 6.6kW and discharge mode is 6.0kW, the switching frequency range is 400~600kHz at full power, the resonant inductor Lr is 6uH and resonant frequency is 290kHz, lower than the switching frequency, ensure the ZVS action of the devices.

TABLE II. Main Parameters of Resonant DAB

	Main parameters	
	Items	***Valus***
Spec. of Bi-DC/DC	V_{Bus} range	360~420V
	V_{HVO} range	550~900V
	Charging power	6.6kW
	Discharging power	6.0kW
	Frequency range	400~600kHz
	Primary side 650V GaN devices	NV6514
	Secondary side 1200V SiC devices	G3R75MT12J
Spec. Resonant tank	Transformer turns ratio	12:20
	Lr	6uH
	Lm	80uH
	Crp/Crs	100nF/300nF
	fr	290kHz

Navitas Semiconductor GaNFast series 650V-25mΩ Toll package NV6514 was selected as the primary side devices, GeneSiC 1200V-75mΩ To-263-7 package G3R75MT12J was selected as the secondary side devices. The curves of Eon and Eoff VS ID currents of NV6514 and G3R75MT12J are shown in Fig. 14. It can be seen that Eon of SiC higher by at least 2 times than GaN, while Eoff by at least 10 times.

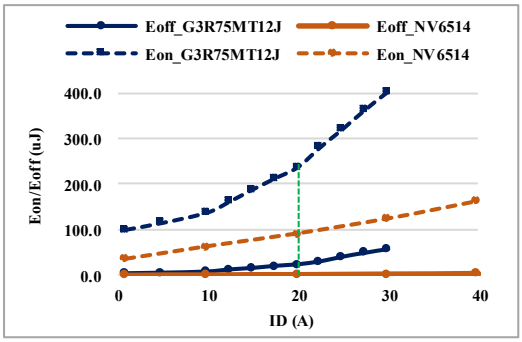

Fig. 14. Eon and Eoff VS ID

For high-frequency ZVS application, it is mainly the turn-off loss, and calculation formula is as follows:

$$P_{Off\_Loss} = E_{Off} \cdot f_s \tag{21}$$

When the turn-off current ID is 20A, the Eoff of G3R75MT12J is 22uJ, when the switching frequency is 500kHz, the calculated loss is 11W. It can be know that as long as the design of turn-off current is below 20A, SiC devices can be safely applied with high frequency design.

A. *Simulation and Loss Breakdown*

Based on the design parameters in Table II, the bidirectional resonant DAB is simulated by SIMetrix-SIMPLIS software. According to the above analysis, the best turn-off current for SiC in high-frequency applications above 500kHz is not more than 20A. The simulation results of the charging mode are shown in Fig. 15. The turn-off current of SiC devices corresponding to the V_{HVO} at 550V and 900V is 3.5A and 17A respectively, and the turn-off current of GaN is 21A and 4.5A respectively. The simulation results of discharging mode are shown in Fig. 16. The turn-off current of SiC devices corresponding to the V_{HVO} at 550V and 900V input is 7.5A and 16A respectively, and the turn-off current of GaN is 17.6A and 1.5A respectively. The turn-off current of charging and discharging mode is within the expected turn-off current range.

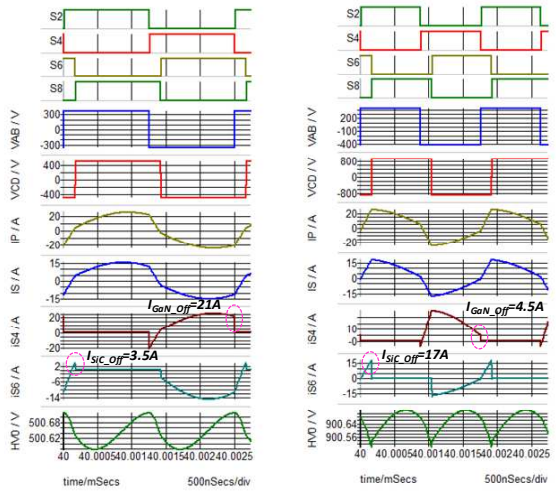

Fig. 15. Charging mode. (a) V_{Bus}=360V, V_{HVO}=550V, fs=400kHz. (b) V_{Bus}=420V, V_{HVO}=900V, fs=570kHz

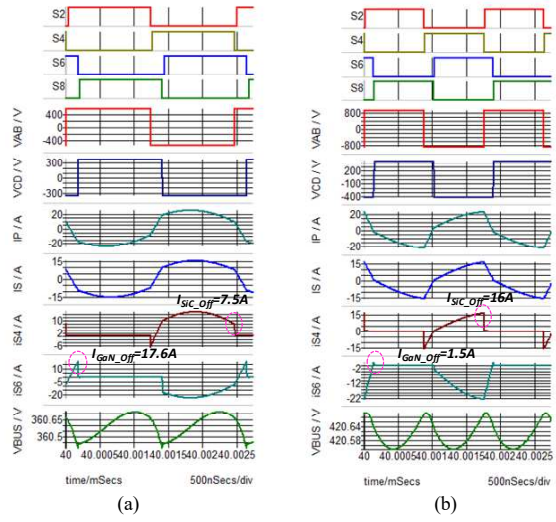

Fig. 16. Discharging mode. (a) V_{HVO}=550V, V_{Bus}=360V, fs=405kHz. (b) V_{HVO}=900V, V_{Bus}=420V, fs=570kHz

To further check the rationality of the design, Fig. 17 respectively gives the loss breakdown and efficiency calculation at 550V_{HVO} and 900V_{HVO} in the worst-case working condition. Due to the fast turn-off speed of GaN and small Eoff value, its turn-off loss is small and can be almost ignored. At the charging mode of 6.6kW and 900V output, 570kHz switching frequency, the turn-off current of SiC is 17A, its loss reaches 10.3W. The transformer loss is obtained based on Maxwell simulation. The final loss breakdown overview, the maximum power loss of GaN device is 13.4W, the maximum loss of SiC device is 15.7W, and the calculated value of efficiency is more than 97.6%.

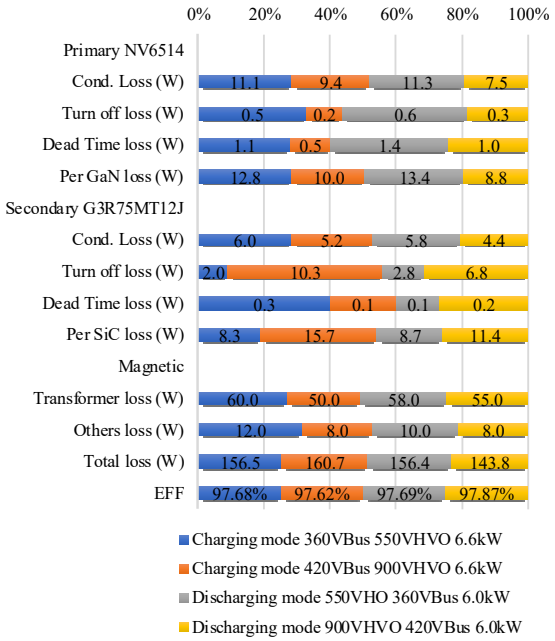

Fig. 17. Loss breakdown of charging and discharging mode

B. *Experimental Verification and Efficiency*

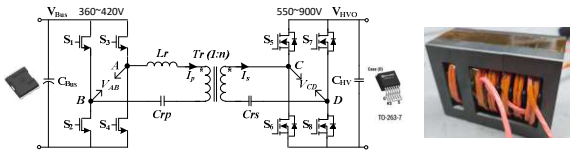

Fig. 18. Power devices and high-frequency transformer

As shown in Fig. 18, the primary side GaN of the resonant DAB topology is Toll package, and the secondary side SiC is To-263-7L package, which is convenient for production and sample making. The high frequency transformer adopts the integrated design of leakage induction add independent inductance, which reduces the volume and improves the power density.

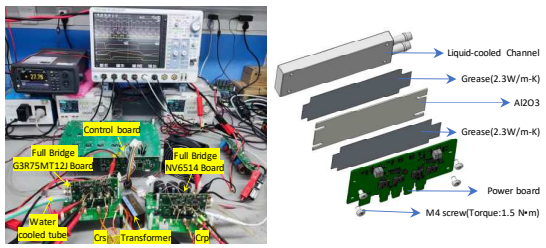

Fig. 19. Experimental platform setup and water-coolant solution

Fig. 19 shows the experimental platform of resonant DAB. A full-bridge evaluation board has been developed for GaN and SiC applications respectively, which is easy to operate. In order to increase the heat dissipation capacity of the device, PCB copper inlay technology is used, combined with ceramic for insulation and heat dissipation treatment, which improves the safety and heat dissipation capacity of the system. The simulation value of the thermal resistance of the system is 2.6℃/W.

Fig. 20 shows the test waveform at 360V V_{Bus} input, 550V V_{HVO} output and 6.6kW P_o in charging mode. The switching frequency is 392kHz, the turn-off current of the primary side GaN device is 20.5A, and the turn-off current of the secondary SiC device is 6.9A.

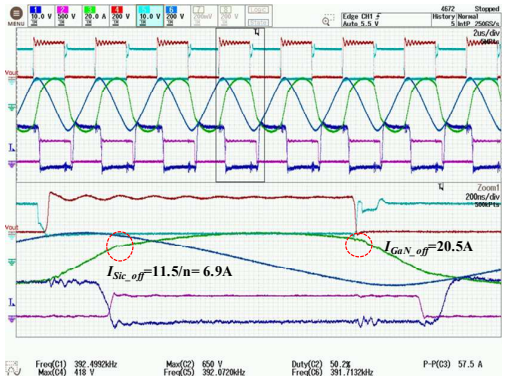

Fig. 20. Charging mode: V_{Bus}=360V,V_{HVO}=550V, P_o=6.6kW and fs=392kHz. (Ch1:Vgs_S_8, Ch2:VDS_S_8, Ch3:Ip, Ch4: VDS_S_2, Ch5: Vgs_S_2, Ch6:VCrp)

Fig. 21 shows the test waveform at 420V V_{Bus} input, 900V V_{HVO} output and 6.6kW P_o in charging mode. The switching frequency is 558kHz, the turn-off current of the primary side GaN device is 8.7A, and the turn-off current of the secondary SiC device is 12.7A.

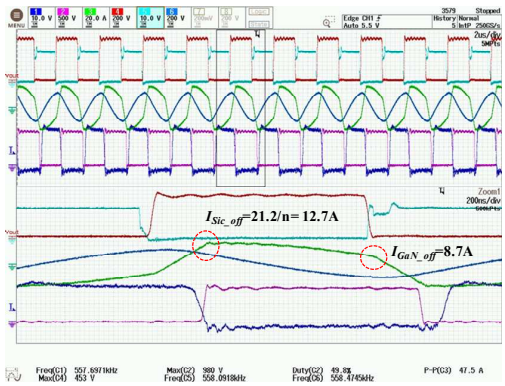

Fig. 21. Charging mode: V_{Bus}=420V,V_{HVO}=900V, P_o=6.6kW and fs=558kHz. (Ch1:Vgs_S_8, Ch2:VDS_S_8, Ch3:Ip, Ch4: VDS_S_2, Ch5: Vgs_S_2, Ch6:VCrp)

Fig. 22 shows the test waveform at 550V V_{HVO} input, 360V V_{Bus} output and 6.0kW P_o in discharging mode. The switching frequency is 405kHz, the turn-off current of the primary side GaN device is 17.4A, and the turn-off current of the secondary SiC device is 7.2A.

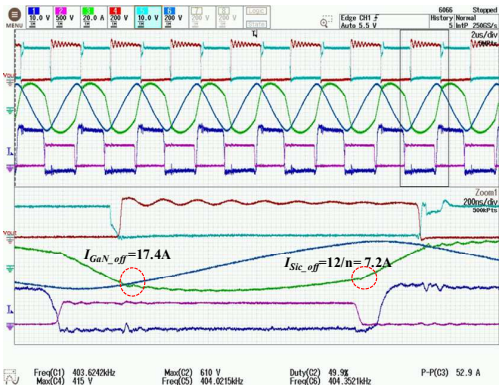

Fig. 22. Discharging mode: V_{HVO}=550V, V_{Bus}=360V, P_o=6.0kW and Fs=405kHz. (Ch1:Vgs_S_8, Ch2:VDS_S_8, Ch3:Ip, Ch4: VDS_S_2, Ch5: Vgs_S_2, Ch6:VCrp)

Fig. 23 shows the test waveforms at 900V V_{HVO} input, 420V V_{Bus} output and 6.0kW P_o in discharging mode. The switching frequency is 565kHz, the turn-off current of the primary side GaN device is 3.5A, and the turn-off current of the secondary SiC device is 12A.

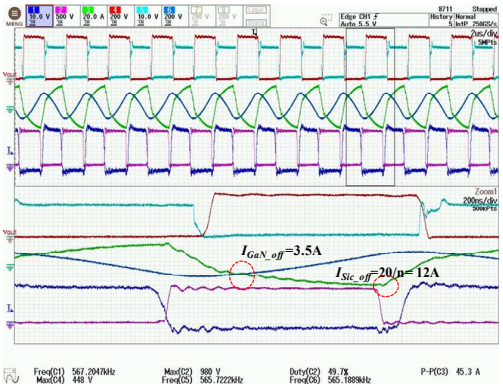

Fig. 23. Discharging mode: V_{HVO}=900V, V_{Bus}=420V, P_o=6.0kW and fs=565kHz. (Ch1:Vgs_S_8, Ch2:VDS_S_8, Ch3:Ip, Ch4: VDS_S_2, Ch5: Vgs_S_2, Ch6:VCrp)

The efficiency curves of 6.6kW charging and 6.0kW discharging mode tested at 25℃ of ambient temperature and water-coolant temperature are shown in Fig. 24. In order to optimize the efficiency, variable Bus voltage control is adopted, V_{Bus} voltage range is 360~420V, and the peak efficiency of charging and discharging is 98.2% and 98.3%, respectively.

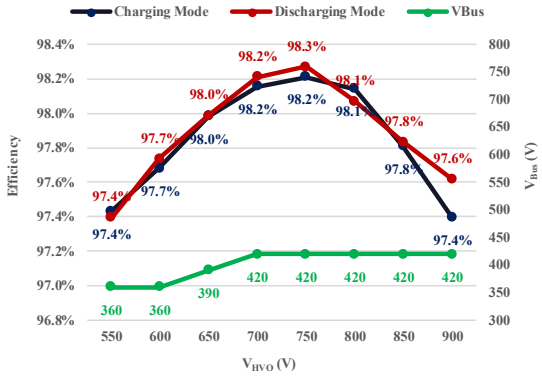

Fig. 24. Efficiency of charging and discharging mod

To reduce reactive power loss of resonant DAB and improve efficiency, SPS closed-loop control is adopted, and the switching frequency is controlled by open loop based on V_{Bus} voltage. Fig. 25 shows the switching frequency curve at the charging and discharging mode of full power. It can be seen that the switching frequency varies narrow between 394kHz and 568kHz, and the switching loss can be controlled within a certain range.

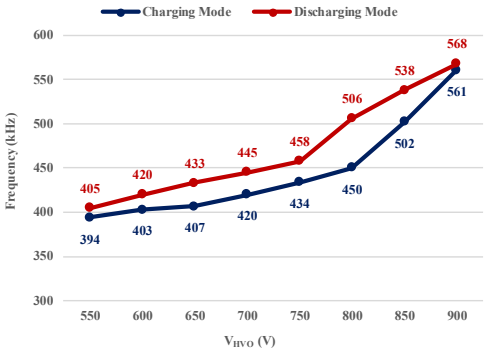

Fig. 25. Switching frequency of charging and discharging mod

C. Discussion

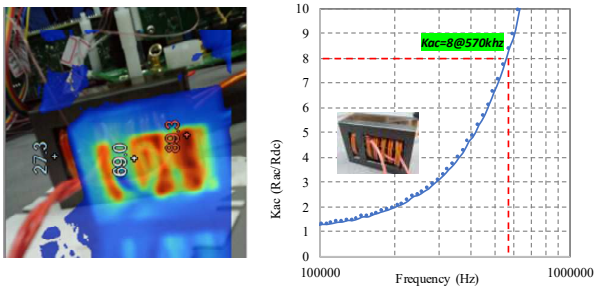

Fig. 26. Transformer thermal and Kac

At present, the product design and application of 500kHz high-power transformers are still rare. The main problem is that with the increase of switching frequency, the resonant current skin effect is enhanced, and the AC loss of transformers winding is approximately exponential. Fig. 26 shows the thermal imaging scanning diagram of the transformer at the charging mode is 6.6kW, 570kHz and the output is 900V. It can be seen that under the condition of normal temperature, the winding temperature is close to 90 ℃. Although 0.05*800 Litz wire is used for winding, the Kac still reaches 8, that is, the impedance of the actual conductor is expanded to 8 times that of the DC impedance. According to the above analysis, engineers in the design of high-frequency transformers, as far as possible to reduce the AC coefficient, and then reduce the AC loss, commonly used measures include the interleaved wiring, the use of Litz wire, etc., to be further studied by scholars.

V. Conclusions and Futuer Work

In this paper, based on the turn-off characteristics of GaN and SiC, resonant DAB is selected for bidirectional DC/DC design, and an integrated high-frequency transformer is designed. Through simulation analysis and experiment, the feasibility of GaN and SiC application in 800V OBCM is verified. In the future, the design of the transformer will be optimized to reduce Kac and winding loss, improve the efficiency of the whole machine, and finally carry out product design to further verify the reliability of the design.

Acknowledgment

The authors would like to thank all the engineers in the Power Electronics Laboratory of Navitas Shanghai Electric Vehicle Team for their help and support.

EFERENCES

[1] Bay, Olcay, et al. "A Comprehensive Review of GaN-Based Bi-directional On-Board Charger Topologies and Modulation Methods." Energies 16.8 (2023): 3433.

[2] Li, Bin , et al. "Bi-directional on-board charger architecture and control for achieving ultra-high efficiency with wide battery voltage range." Applied Power Electronics Conference & Exposition IEEE, 2017.

[3] Ammar, Ahmed M. , K. Ali , and D. J. Rogers . "A Bidirectional GaN-Based CLLC Converter for Plug-In Electric Vehicles On-Board Chargers." IECON 2020 - 46th Annual Conference of the IEEE Industrial Electronics Society IEEE, 2020.

[4] He, Peiwen , et al. "Design of a 1-MHz High-Efficiency High-Power-Density Bidirectional GaN-Based CLLC Converter for Electric Vehicles." IEEE Transactions on Vehicular Technology (2018):1-1.

[5] Shahed, Md Tanvir, and ABM Harun-Ur Rashid. "Wide bandgap semiconductor based high performance bidirectional resonant converter for electric vehicle application." 2022 International Conference on Advancement in Electrical and Electronic Engineering (ICAEEE). IEEE, 2022.

[6] Gang, Liu , et al. "Implementation of a 3.3-kW DC–DC Converter for EV On-Board Charger Employing the Series-Resonant Converter With Reduced-Frequency-Range Control." IEEE Transactions on Power Electronics 32.6(2017):1-1.

[7] Minli, Jia, and Sun Hao. "GaN-based High Frequency 6.6 kW Bi-directional DC/DC Converter for OBC Application." 2022 IEEE International Power Electronics and Application Conference and Exposition (PEAC). IEEE, 2022.

[8] Zhao, Biao , et al. "Overview of Dual-Active-Bridge Isolated Bidirectional DC–DC Converter for High-Frequency-Link Power-Conversion System." IEEE TRANSACTIONS ON POWER ELECTRONICS PE 29.8(2014):4091-4106.

[9] Li, X. , and A. K. S. Bhat . "Analysis and Design of High-Frequency Isolated Dual-Bridge Series Resonant DC/DC Converter." IEEE TRANSACTIONS ON POWER ELECTRONICS PE 25.4(2010):P.850-862.

[10] Hu, Song , X. Li , and Q. Zheng . "A Dual-Bridge DC/DC Resonant Converter Using Extended PWM and Phase-shift Control." IEEE Transactions on Industry Applications PP.99(2021):1-1.

[11] Ouyang, Ziwei, Ole C. Thomsen, and Michael AE Andersen. "Optimal design and tradeoff analysis of planar transformer in high-power DC–DC converters." IEEE Transactions on Industrial Electronics 59.7 (2010): 2800-2810.

[12] Zhang, Yanjun, et al. "1MHz-1kW LLC resonant converter with integrated magnetics." APEC 07-Twenty-Second Annual IEEE Applied Power Electronics Conference and Exposition. IEEE, 2007.

[13] Noah, M. , et al. "Winding orientation method to minimize the secondary leakage of a gapped transformer utilized in LLC resonant converter." Institution of Engineering and Technology 3(2018).

[14] Hoang, K. D. , and J. Wang . "Design optimization of high frequency transformer for dual active bridge DC-DC converter." International Conference on Electrical Machines IEEE, 2012.

[15] Liu, Gang, et al. "Bidirectional CLLC resonant DC-DC converter with integrated magnetic for OBCM application." 2015 IEEE International Conference on Industrial Technology(ICIT). IEEE, 2015